THE PENNSYLVANIA STATE UNIVERSITY
SCHREYER HONORS COLLEGE

DEPARTMENT OF ASTRONOMY & ASTROPHYSICS

INVESTIGATING NORMAL STAR-FORMING GALAXIES AT Z $\sim$ 1

Can Cui
Spring 2014

A thesis
submitted in partial fulfillment
of the requirements
for baccalaureate degrees
in Astronomy & Astrophysics and Physics
with honors in Astronomy & Astrophysics

Reviewed and approved* by the following:

Robin Ciardullo
Professor of Astronomy & Astrophysics
Thesis Supervisor

Jane Charlton
Professor of Astronomy & Astrophysics
Honors Adviser

*Signatures are on file in the Schreyer Honors College.

Abstract

We use the 3D-HST visible and near-IR grism survey to study the star formation rate (SFR), stellar mass and extinction with normal star-forming galaxies selected in the GOODS-South region in the redshift ranges $0.68<z<0.82$ and $1.2<z<1.4$. These spectra include the emission lines of Hα, Hβ, [O III] 5007, and [O II] 3727. For our sample, we find the correlation between nebular extinction derived from balmer decrement and stellar extinction from SED fitting agrees with the z $\sim$ 0 universe, which has an empirically correlation that the extinction for nebular lines is $\sim$ 2 times that found from the star light. Some of our sample contain high [O III]/Hβ ratios which we think could be due to high-energy photons emitted from AGN, shocks from winds, or hot stars.

Table of Contents

List of Figures

Acknowledgements

I would wish to thank Dr. Robin Ciardullo, my research and thesis supervisor, for his encouragement, guidance, and support on this project and my graduate school application.

Much gratitude is extended to Dr. Greg Zeimann for his mentorship throughout my year on this project and for his unstinting help on everything. Without his help this whole project would not have been possible. I deeply appreciate this. I also want to thank Joanna Bridge as she has been so industrious on providing me the data and measurements for this project. Thanks for everyone in our HETDEX group, it has been such a pleasure to work with all you guys for the year.

I am also indebted to Dr. Don Schneider for introducing me to the magic of the universe through his fantastic classes as well as for his care and encouragement on my study, research and graduate school application.

I would also like to thank my honors advisor (in Astronomy) Dr. Jane Charlton for her support throughout the project. I owe a debt of gratitude to Dr. Richard Robinett for being the best academic advisor (in Physics) I could have ever hoped for.

Last but not least, I would like to thank mum and dad for their unwavering support forever.

Chapter 1

Introduction

The first galaxies were created when the Universe was a few 100 million years old (Bromm & Yoshida, 2011). The most current study estimates that there are several hundred billion galaxies in the Universe (NASA, 2014). Despite their ubiquity, the theory of the evolution of galaxies is still not complete. One key question is to understand the star formation rate (SFR) of galaxies, which is a crucial characteristic to describe galaxy star formation history.

Regardless of the unsophisticated instruments and limited information of the evolutionary histories of galaxies, the studies by Tinsley, 1968, 1972 and Searle et al., 1973 first derived the SFRs quantitatively and led to the prediction of the cosmic star formation history. Powerful facilities over the past decade such as the new instruments on the *Hubble Space Telescope (HST)*, the *Galaxy Evolution Explorer (GALEX)*, the *Spitzer Space Telescope* and the *Herschel Space Observatory*

have provided new observational information on star formation and hence extended the diagnostic methods for measuring SFRs in galaxies.

Many calibrations of SFR depend on the luminosity measured at various wavelengths including ultraviolet, infrared, optical, radio and X-ray. Ultraviolet continuum emission (Kennicutt & Evans, 2012) is one of the most popular tracers of the SFR, which directly traces the photospheric emission of young stars. *GALEX* has had a significant impact on ultraviolet this subject by providing integrated ultraviolet fluxes for numerous numbers of relatively nearby galaxies. Another essential method for deriving a complete star formation history is based on the infrared emission, since half of the light from stars is absorbed by interstellar dusts and re-emitted in the infrared. Moreover, the centimeter-wavelength radio continuum emission of galaxies provides a photoionization-based measure of the SFR without encountering the issue of dust attenuation. And over the past decade, the integrated hard X-ray emission of galaxies has become a new tracer on account of its close association with young stellar populations and recent star formation.

The Hα emission line is the most widely applied diagnostic of measuring current SFR in galaxies and understanding the cosmic star formation history. All hydrogen atoms in the ISM are in their ground state since the ISM is clod and collisions are rare. Photons with energy equal or higher than 13.6 eV from young hot stars ionize neutral hydrogen, and these ionized hydrogen will recombine with electrons. The photons generated from electrons transit to n=1 are quickly re-absorbed by nearby neural hydrogen atoms. This CASE B recombination causes every recombination eventually resulting in a transition to n=2 (Balmer series). By measuring Hα emission line, we can determine the total amount of ionizing photons, hence the number of young stars as well as star formation

In my research, we study the star formation history by selecting a sample of distant Hα-

emitting galaxies based on the data from the 3D-HST survey (Brammer et al., 2012). The 3D-HST slitless grism survey provides deep imaging and grism spectroscopy datasets of the well-studied extragalactic fields. we focus on the GOODS-South region containing both WFC3/G141 and ACS/G800L grism. Through reducing ACS slitless spectroscopic data and identifying the Hα-emitting galaxies, we measure star formation rate through Hα emission, stellar mass through spectra energy distribution fitting, extinction due to dust through the Balmer decrement, and oxygen abundance through empirical relations. By comparing these Hα-emitting galaxies with more local galaxies, models of galactic chemical evolution can be tested.

Chapter 2

The *HST* Data and Reductions

2.1 Optical/Near-IR Imaging

To perform the analysis, we take advantage of the original optical images of the GOODS-S field from 3D-HST and the corresponding deep, multi-color optical and near-IR photometry from the CANDELS survey (Grogin et al., 2011, Guo et al., 2013).

2.2 The *HST* Spectroscopy

Two surveys from the 3D-HST (Brammer et al., 2012, GO-12177), a near-IR grism survey with the *HST* 's WFC3 camera and an optical grism survey with *HST* 's ACS camera, provide the rest-frame optical emission-line measurements for the analysis. These two surveys were opti-

mized to maximize the overlap between WFC3 and parallel ACS observations. The WFC3 field observed with the G141 grism consists of 46.5 Å/pixel (R $\sim$ 130) slitless spectroscopy between 10800Å $< \lambda <$ 16800Å, which covers $\sim$ 80% of the area imaged by the CANDELS survey. The ACS field observed with G800L grism consists of 40 Å/pixel, 80 Å of resolution slitless spectroscopy between 5800Å $< \lambda <$ 9500Å , which includes $\sim$ 95% of the CANDELS footprint. Strong emission lines in the redshift ranges $0.68 < z < 0.82$ and $1.2 < z < 1.4$ fall onto both G141 and G800L grism. For $0.68 < z < 0.82$, G141 grism covers Hα, [N II] $\lambda\lambda$6548, 6584, [S II]$\lambda\lambda$6716, 6731, and G800L grism covers [O II] λ3727, Hβ, [O III] $\lambda\lambda$4959, 5007. For $1.2 < z <$ 1.4, G141 grism covers Hβ, [O III] $\lambda\lambda$4959, 5007, Hα, [N II] $\lambda\lambda$6548, 6584, [S II]$\lambda\lambda$6716, 6731, and G800L covers [O II] λ3727.

To reduce these data, we began with the pre-processed, calibrated "FLT" files for WFC3 and "FLC" files for ACS in the *HST* Data Archive."FLC" files only differ from "FLT" files in that they include a correction for charge transfer inefficiencies that now commonly occur in ACS observations. "FLT" and "FLC" files are the products of the automated reduction process calwfc[1] and calacs[2], respectively. These two reduction processes use the latest reference files to measure and subtract the bias, correct for non-linearity, flag saturated pixels, subtract the dark image, divide by the flatfield, calculate the gain, and apply the flux conversion. This process was identical for both the direct and the grism images, except that for the flat fielding step, the grism data were flat fielded at a later stage using the aXe[3] software and a master sky flat.

For slitless spectroscopy, each direct image is accompanied with a grism image to calibrate wavelength and properly identify and extract spectra.To determine the location of the spectra in

[1]http://www.stsci.edu/hst/wfc3/documents/handbooks/
[2]http://www.stsci.edu/hst/acs/documents/handbooks/
[3]http://axe.stsci.edu/

the grism image and define extraction parameters, we used the positions and the size of the objects detected in the direct image. The direct images were reduced using MultiDrizzle software (Fruchter et al., 2009) which produced a distortion-corrected, cosmic-ray rejected, coadded image for each observation. The direct images we used in F140W are $\sim$200s individual exposures, taken in a 4 exposure dither pattern (Brammer et al., 2012). With the deeper CANDELS imaging (as described in Zeimann et al., 2014), we extracted objects down to a magnitude of 26 AB. The direct imaging in F814W was deep enough to extract sources down to 25 AB. We used the position of the sources in a master catalog extracted by SExtractor (Bertin & Arnouts, 1996). The grisms were extracted separately, and positionally matched in catalog space with a matching radius of X arcsec.

Very similar to the grism reduction steps described in the WFC3 Grism Cookbook[4] and ACS Data Handbook[5], both the G141 and the G800L grism data were reduced using the program aXe[6] version 2.3 (Kümmel et al., 2009). First, the task AXEPREP was used to subtract the latest and best master sky frame[7] from each image; such a step is critical for the extraction of the faintest targets. Although the best fit is using a full set of master sky images since the background of a grism image is variable over time, small variations in continuum levels are not a serious issue when we are solely concerned with the detection and measurement of emission lines.

After subtracting the sky, we began to extract the 2-D spectrum of each individual object in the master SExtractor catalog. This was done using AXECORE, which defines each source's extraction geometry, flat-fields the region containing the spectral information, applies the wavelength calibration, and determines the contamination from overlapping spectra. Each object was traced with a variable aperture based on its size on the direct image ($\pm$4 times the projected width of

[4]http://www.stsci.edu/hst/wfc3/analysis/grism_obs/cookbook.html
[5]http://www.stsci.edu/hst/acs/documents/handbooks
[6]http://www.stsci.edu/institute/software_hardware/stsdas/axe/
[7]http://www.stsci.edu/hst/wfc3/analysis/grism_obs/calibrations/wfc3_g141.html

the source in the direction perpendicular to the spectral trace). Objects present on multiple frames were then run through DRZPREP and AXEDRIZZLE, which rejected the cosmic rays, drizzled the data to a common system (Fruchter et al., 2009), and co-added the images into one higher signal-to-noise 2-D spectrum. Finally, 1-D spectrum for each object with flux, error on the flux, and a contamination fraction in units of flux was created using the optimal extraction method discussed by Kümmel et al. (2009).

To summarize the whole reduction process, we created a webpage combining the 2-D grism images with the 1-D extracted spectra for visual convenience. This was done with an input catalog and the aXe output files to create a summary of the full reduction by the program aXe2web[8]. On the webpage, each object is displayed on a separate row with columns arranged in the order of its corresponding magnitude, (x, y) position, equatorial coordinates, direct image cutout, grism image cutout, and 1-D extracted spectrum in counts and flux. This webpage is well designed with a visually useful format to view a summary of the reductions, maintain quality control, and select sub-samples of objects for science purposes.

[8]http://axe.stsci.edu/axe/axe2web.html

Chapter 3

Sample Selection and Measurements

3.1 Matching Sources in the G800L and G141

We began the process of sample selection by matching the objects distributed in both the WFC3 and ACS field. We matched sources from the two different grisms using a 1 arcsec separation. This separation was chosen to minimize false matches while still allowing for small deviation due to astrometric offsets. Using the matched catalogs, we adjusted the webpage output of aXe2web to display the combined 1-D extracted spectra from the G800L and G141 grism for visual inspection (Seen in FIG. 3.1).

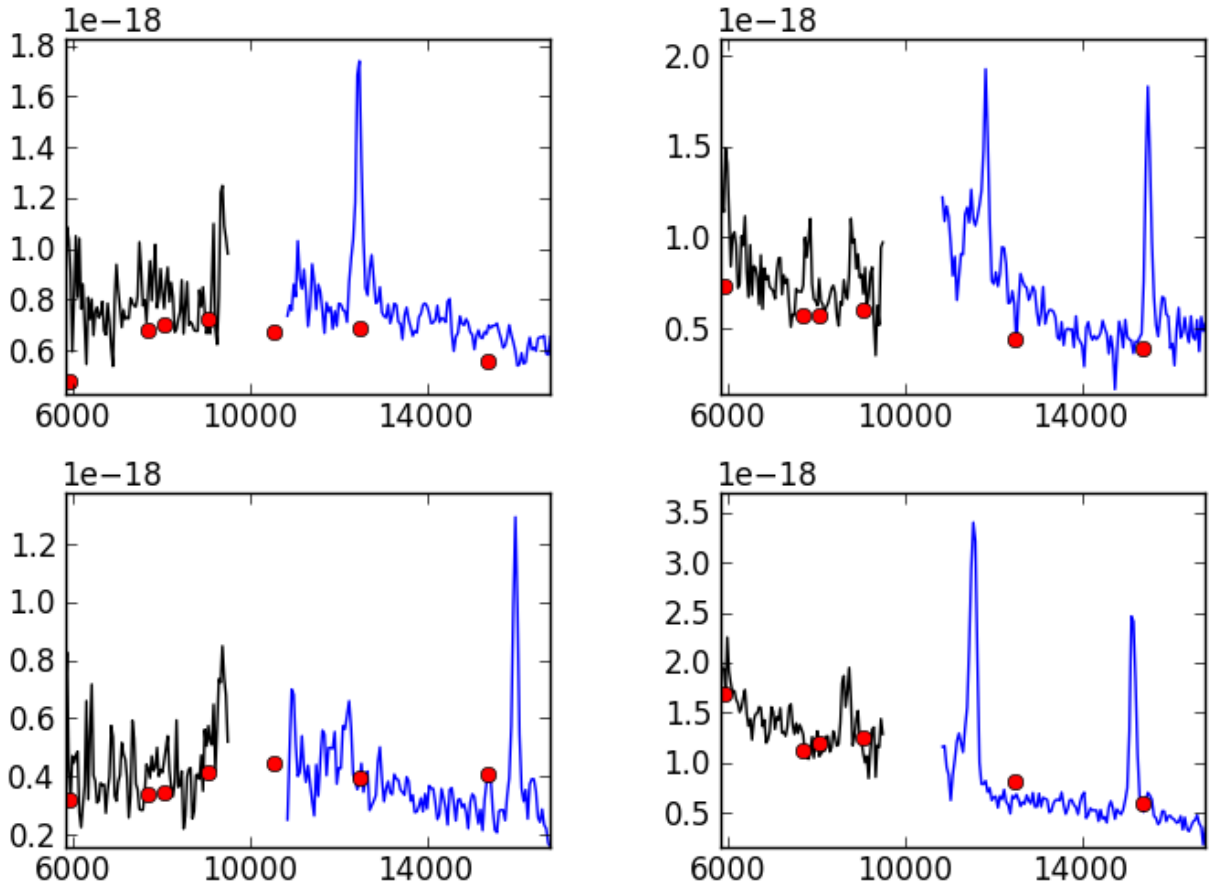

Figure 3.1: Sample combined 1-D extracted spectra. The black lines show the flux measured from G800L grism, and the blue lines show the flux measured from G141 grism. The red dots are plotted using the CANDELS photometry. The x-axis measures the wavelength and the y-axis measures the flux. Strong Hα line is accompanied with weaker [S II]$\lambda\lambda$6716, 6731 line on the right while strong [O III]$\lambda\lambda$4959, 5007 line is accompanied with weaker Hβ on the left.

3.2 Selecting Samples by Hα, [O III] and Hβ

We examined the combined spectra for Hα+[N II], Hβ, [O II] λ3727, and [O III] $\lambda\lambda$4859, 5007. The redshifts $0.68 < z < 0.82$ and $1.2 < z < 1.4$ were the ideal redshift ranges for selection because the bright lines of Hα+[N II], Hβ, [O III] and [O II] all fall within the coverages of both the G141 and G800L grisms . Specifically, the emission line of Hα+[N II] in the wavelength ranges 11000Å $< \lambda <$ 12000Å and 14400Å $< \lambda <$15800Å was the most preferred feature for selection

because it is typically the strongest emission line seen in the combined 1-D spectra. If multiple emission lines provided a consistent redshift in the two ranges above, then the object was selected for our sample.

3.3 Measuring Flux, Luminosity and SFR

To measure fluxes of different emission lines, we used Gaussian emission models and polynomial continuum. Initially, we measured the redshift of each source by hand. The wavelength calibration of our grism spectra depended on the centering of the object in the direct image. If the centroid of a source in the F814W image was slightly offset ($\sim$1 pixel) from the source's centroid in the F140W image, then the relative wavelength calibration of the G800L and G141 grism might be offset by $\sim$40-45 Å. To account for this, we determined a slightly different, separate redshift for the G800L and G141 grisms. We also defined three small windows ($\Delta\lambda \sim 900$Å) encompassing [O II], Hβ and [O III], and Hα and [S II] to fit Gaussian emission models and a linear continuum. In each window, we restricted the Gaussians to the same width, but allowed a small amount of wiggle room for the centroiding. Approximately 20% of the time, however, contamination from overlapping spectra significantly affected the flux measurement process. When this was the case, we eliminated the source from our sample. To calculate the error of fluxes, we assumed that the uncertainties for each data point in the spectrum form a Gaussian distribution. By bootstrap resampling, we resampled the data points 1000 times and refit. The 16th and 84th percentiles of the resulting distributions were taken to be the error for each flux measurement. As seen in FIG. 3.2, the fluxes of Hα emission lines measured from our sources are in the range of $\sim 10^{-15} - 10^{-17}$ erg/s/cm^2.

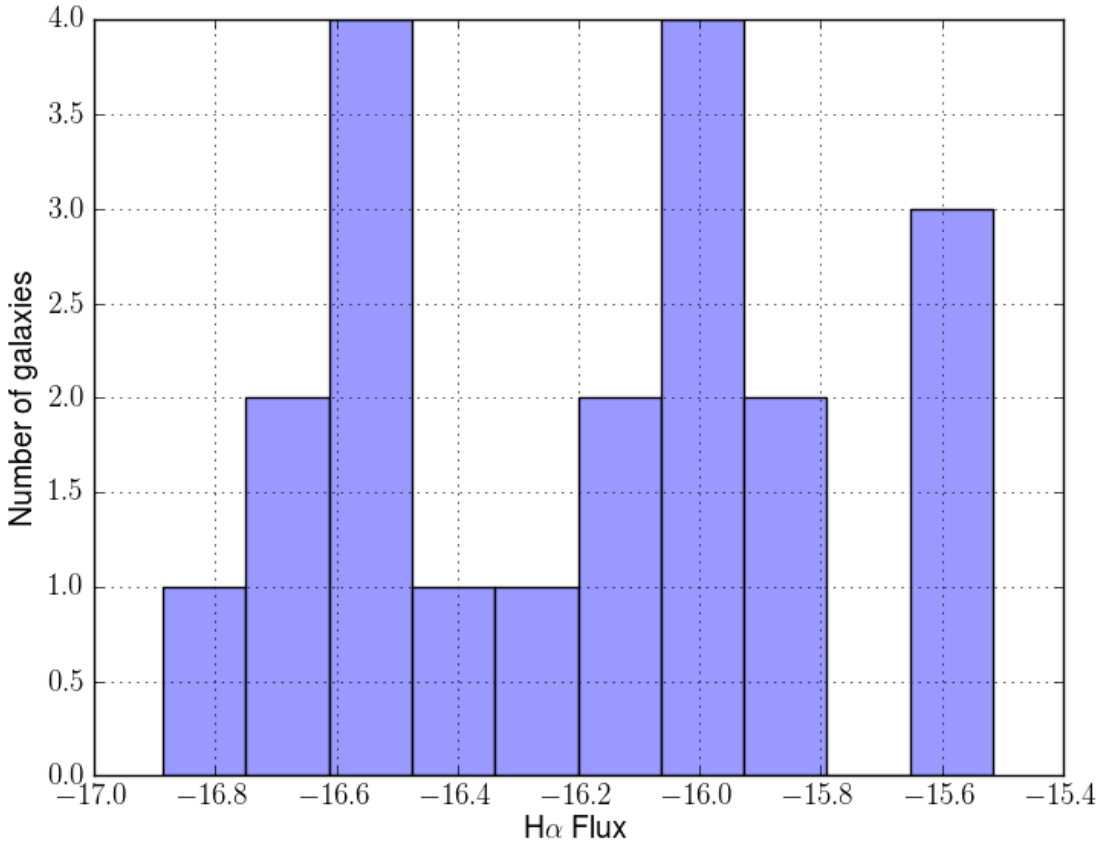

Figure 3.2: The histogram of Hα flux and corresponding number of galaxies. The fluxes of Hα emission lines measured from our sources are in the range of $\sim 10^{-15} - 10^{-17}$ erg/s/cm^2.

To convert flux into luminosity, we adapted the standard cosmological model (ΛCDM model) to determine the luminosity distance for our sources. The standard model suggests a dark energy density $\Omega_\Lambda \sim 0.7$, a matter density (baryon+dark matter) $\Omega_\mathrm{M} \sim 0.3$, and a third density to measure the curvature of space $\Omega_k \sim 0$. Based on the standard cosmological model, the comoving distance and the luminosity distance are determined using Hogg (1999). Using the luminosity distance, the luminosity is simply obtained from the flux.

As we discussed in the introduction, Hα photons are produced during the recombination process by young OB stars in star-forming galaxies. The number of hydrogen ionizing photons and the luminosity of Hα are directly correlated (Kennicutt, 1998, Kennicutt & Evans, 2012) for an photoionization environment which is optically thick to Lyman photons but thin for higher order series (Balmer, Paschen, etc.). Massive stars are presumed as the source of ionizing photons since massive stars are hot with T>30,000 K, hence they emit high energy photons. For a given star formation rate, the number of ionizing photons can be calculated as a function of the stellar population's age through stellar population modeling, which includes assumptions of how many massive stars there are compared to lower mass stars (IMF), the evolution of a star given a mass, and the composition of the stars (i.e metallicity). For timescales of $>10^7$ years, we assumed the stellar population does not vary too much because massive stars have short lifetimes, and the new massive stars that are born replace the old massive stars that die. With the assumption of solar abundance and using the IMF, the correlation between SFR and Hα luminosity is derived as SFR ($\mathrm{M_\odot\ yr^{-1}}$) $= k \cdot L_{H\alpha}(\mathrm{erg\ s^{-1}})$, where $k = 5.42 \times 10^{-42}$ by Kennicutt & Evans (2012).

One of the issues with respect to calculating SFR from Hα luminosity is that Hα is blended with the [N II] doublet at 6549Å and 6585Å due to the limited resolution of WFC3 G141 grism. To measure only Hα flux, we assumed a ratio of [N II]/Hα = 0.2 as this is a common value among

local galaxies and subtract the blended line off. Another issue related to Hα luminosity is that it will be underestimated if we do not correct for the underlying stellar absorption. The effect of stellar absorption in our selected sources is trivial because the sources contain high equivalent widths (EW), and the relation between true EW and measured EW is $\mathrm{EW_{true}} \sim \mathrm{EW_{meas}} + 2\text{Å}$ (Groves et al., 2012).

We used the Balmer decrement (the ratio of Hα/Hβ) to correct for extinction due to dust, which obscures the intrinsic luminosity of our sources. From Osterbrock & Ferland (2006), the ratio of Hα to Hβ is 2.86 and the ratio maintains in many conditions with different temperature and electron density. The blue light tends to be more obscured than the red light because it has larger cross section with dust than the red light. We related the color excess from extinction to the observed Hα to Hβ ratio by the extinction curve from Calzetti et al. (2000):

$$E(B-V) = \frac{-2.5 \log_{10}{}^{(H\alpha/H\beta/2.86)}}{(k6563 - k4861)} \tag{3.1}$$

By the color excess from extinction, we corrected Hα observed luminosity to its intrinsic value and converted this intrinsic value to SFR. This method is quite accurate when $E(B-V) > 1$.

3.4 Measuring Stellar Mass from SED Fitting

To obtain the stellar mass, we used the GalMC SED fitting code based on the stellar population models of Bruzual & Charlot (2003) updated in 2007. We assumed a constant star formation history, an IMF with $\mathrm{M_L} = 0.1\mathrm{M_\odot}$ and $\mathrm{M_U} = 100\mathrm{M_\odot}$, a Calzetti extinction law (Calzetti et al., 2000), and a fixed metallicity at solar. The GetDist software from Lewis & Bridle (2002) was

used to analyze the chains and test for convergence by the R statistic Gelman & Rubin (1992). Moreover, we adapted $R - 1 < 0.2$ (Acquaviva et al., 2011) and excluded seven objects with less than five photometric bands from the sample to ensure robust SED fits. Sample SED fittings are shown in figure 3.3. We show the SFR versus stellar mass in Figure 3.4.

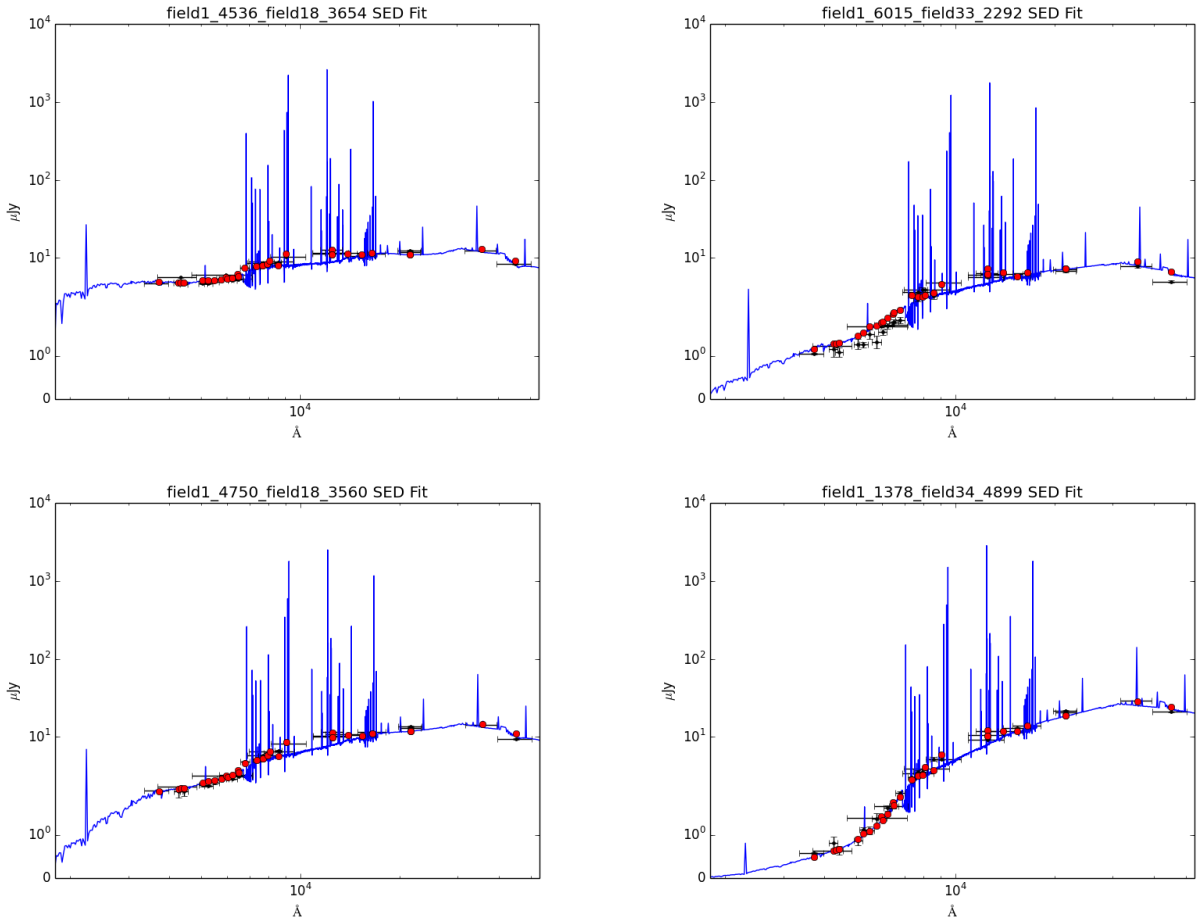

Figure 3.3: Sample SED fittings in the first field of G800L grism. The x-axis is the wavelength and the y-axis is the flux density. Blue lines shows the modeled emission lines, the black points are the photometry in 36 bands, and the red points are the fitted SED flux densities.

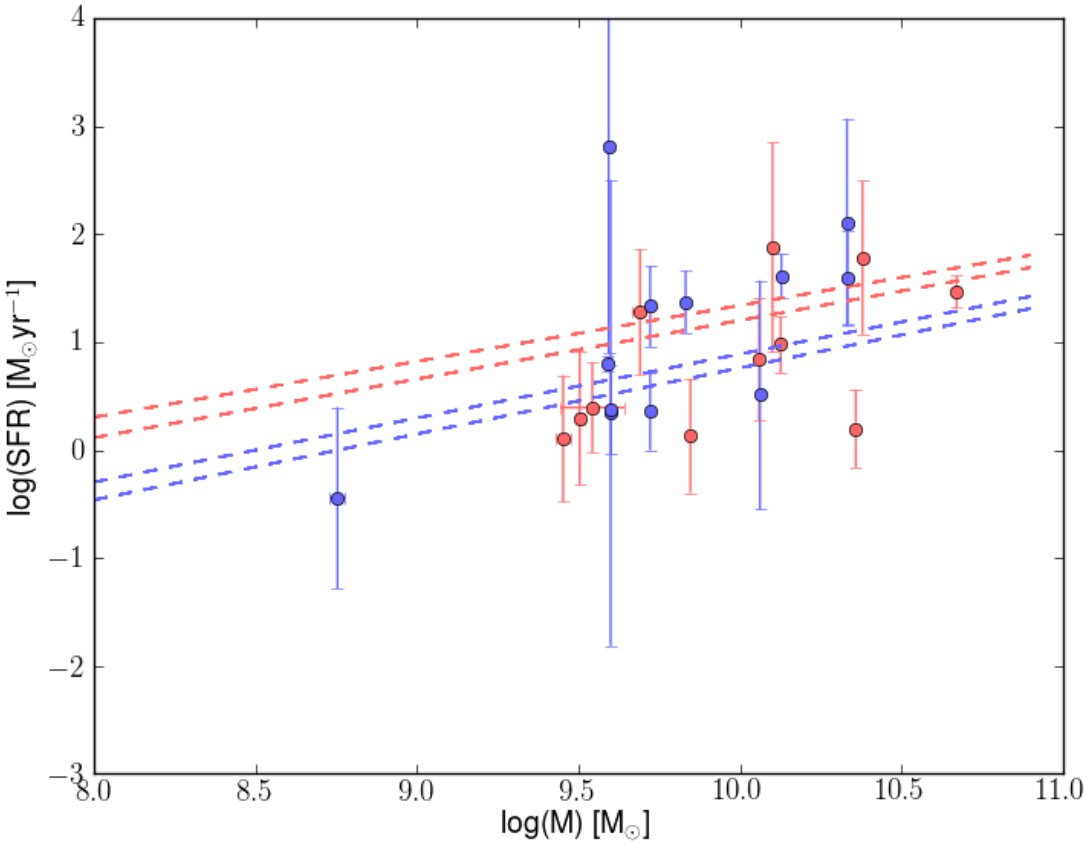

Figure 3.4: SFR versus Stellar Mass for galaxies with redshifts 0.68<z<0.82 and 1.2<z<1.4. The dashed lines are the empirical power law fit for normal galaxies (Whitaker et al., 2012), z=0.68 and 0.82 for blue lines and z=1.2 and 1.4 for red lines. Data points far above the lines are considered as starburst galaxies and far below the lines are passive galaxies. Our samples scatter around the lines which indicates they are normal galaxies.

Chapter 4

Results

4.1 Nebular Extinction vs. Stellar Extinction

Nebulae collapses into filaments and forms stars causing these new-formed massive stars surrounded by dense molecular clouds and dusts (Lada & Lada, 2003). We expect higher extinction for the emission lines from the nebular gas than the other regions in the galaxy. To investigate this theory, we compare the extinction of nebular lines and that of the stellar spectrum. Calzetti et al. (2000,2001) empirically demonstrated for local galaxies ($z \sim 0$) the extinction for nebular lines (i.e. balmer decrement) is $\sim$2 times higher than the extinction found from the star light (i.e. SED fitting). Seen in FIG. 4.1, our samples suggests agreement with the $z \sim 0$ universe. We are working on executing accurate error bars, which will enable us to draw better conclusions. Some

of the samples contain negative nebular extinction due to the stronger Hβ lines than we expected.

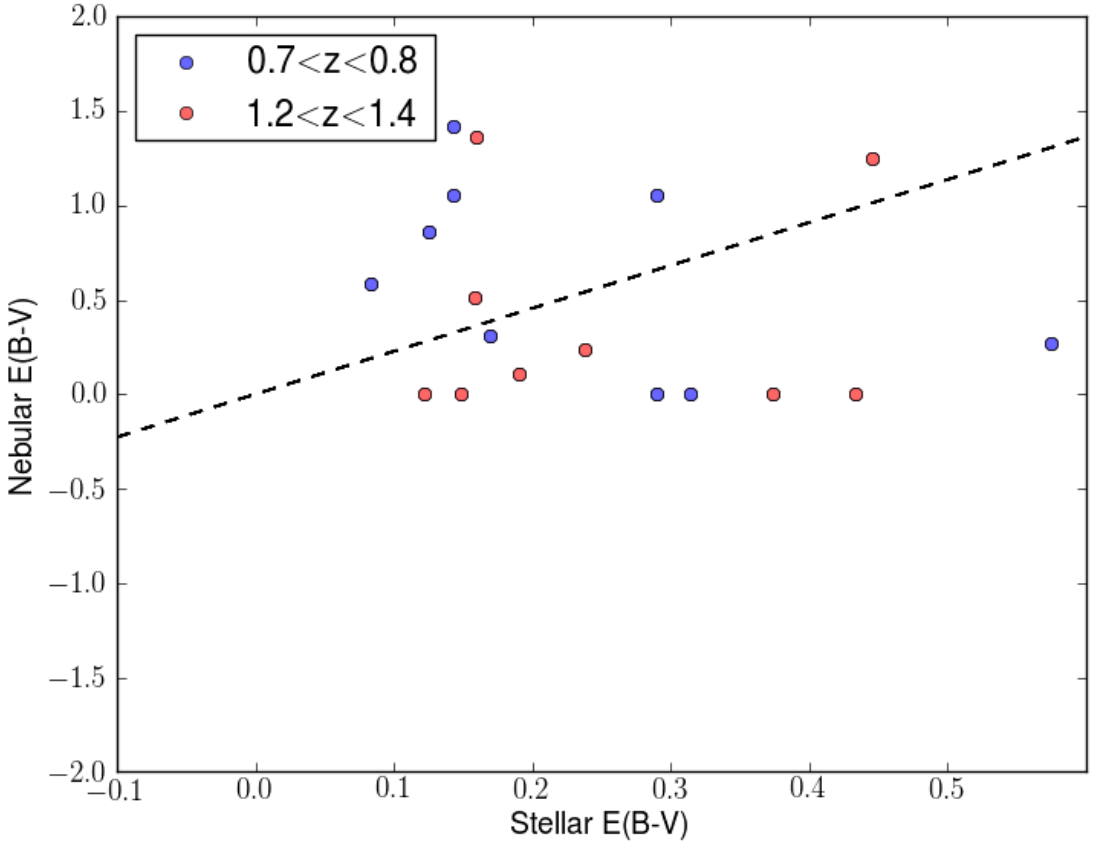

Figure 4.1: Nebular extinction determined with balmer decrement versus stellar extinction with SED fitting. The black line shows the empirical correlation between nebular extinction and stellar extinction (Calzetti et al., 2000, Calzetti, 2001). Our samples scattering around the line suggests agreement with the z $\sim$ 0 universe.

4.2 SFR vs. AGN

we plotted [O III]/Hβ and stellar mass for our samples in FIG. 4.2. Higher stellar mass indicates higher Oxygen abundance, better cooling process, hence lower [O III] to [O II] ratio, which explains the curve drops as the stellar mass increases. We are not sure the data points above the

curve are all AGNs since our sample is in the different redshift ranges than the local galaxies. The high [O III] to Hβ ratio from these galaxies could be also due to shocks from winds or hot stars.

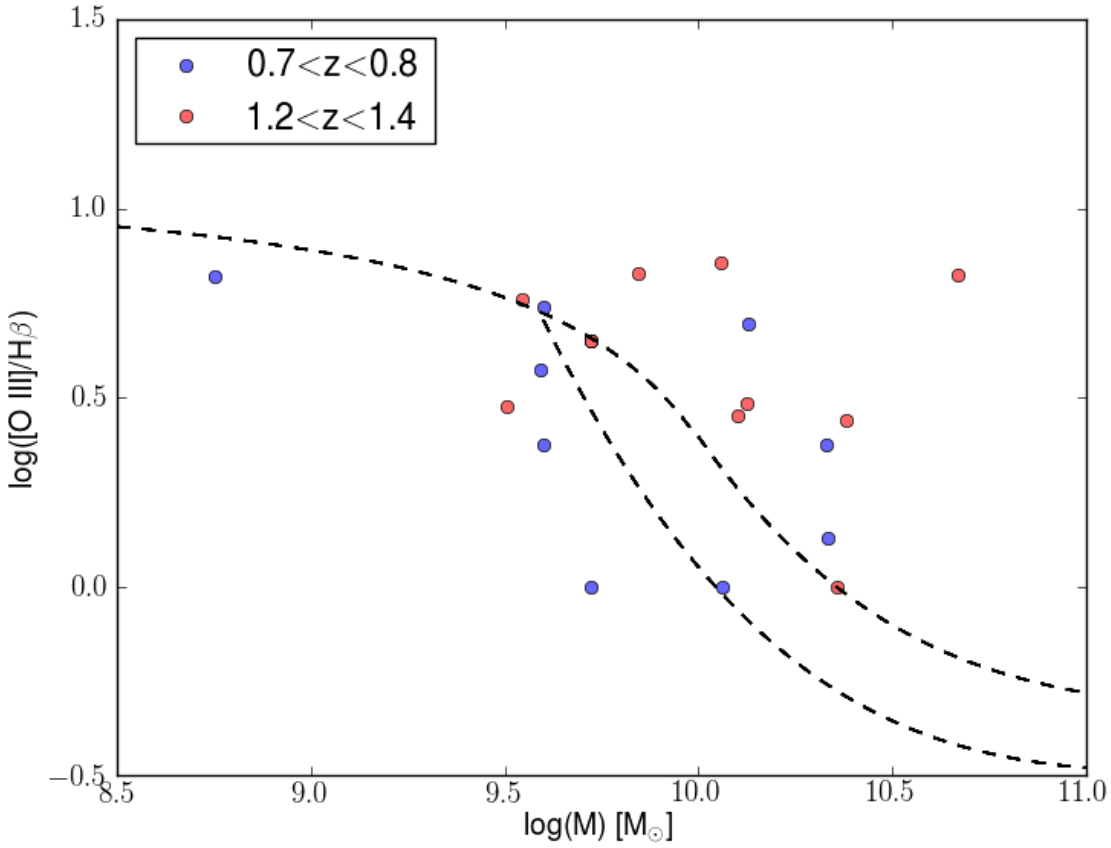

Figure 4.2: [O III]/Hβ versus stellar mass for our sample. The curve demarcates AGN and star-forming galaxies based on the local measurements; data points above the upper curve have a high possibility to be AGN, data points below the lower curve is more likely to be a star-forming galaxy (Juneau et al., 2014). The transition region in between the upper and lower curve indicate an equal probability of being an AGN or normal star formation.

4.3 Future Plans

The preliminary results shown in this paper only included the data from 6 out of more than 30 fields in GOODS-S region. Given time, we will obtain 25 times more data points from the

remaining fields and test if the results are consistent with those we have now. We can also take the advantage of the 2-D spectra to determine line ratios of nuclear region and the outskirts of galaxies to eliminate the effects by AGN. Moreover, we would like to obtain higher spectral resolutions in the future will allow us to avoid blended lines of Hα and [N II] doublet, and thus measure Hα luminosity more accurately.

Bibliography

Acquaviva, V., Gawiser, E., & Guaita, L. 2011, ApJ, 737, 14

Bertin, E., & Arnouts, S. 1996, A&AS, 117, 393

Brammer, G. B., van Dokkum, P. G., Franx, M., et al. 2012, ApJS, 200, 19

Bromm, V., & Yoshida, N. 2011, ARA&A, 49, 373

Bruzual, G., & Charlot, S. 2003, Monthly Notices of the Royal Astronomical Society, 344, 1000

Calzetti, D. 2001, The Publications of the Astronomical Society of the Pacific, 113, 1449

Calzetti, D., Armus, L., Bohlin, R. C., et al. 2000, ApJ, 533, 682

Fruchter, A., Sosey, M., Hack, W., et al. 2009, The MultiDrizzle Handbook, version 3.0, (Baltimore, STScI)

Gelman, A., & Rubin, D. B. 1992, Statistical Science, 7, 457

Grogin, N. A., Kocevski, D. D., Faber, S. M., Ferguson, H. C., & Koekemoer, A. M. 2011, ApJS, 197, 35

Groves, B., Brinchmann, J., & Walcher, C. J. 2012, Monthly Notices of the Royal Astronomical Society, 419, 1402

Guo, Y., Ferguson, H. C., Giavalisco, M., et al. 2013, ApJS, 207, 24

Hogg, D. W. 1999, arXiv:astro-ph/9905116

Juneau, S., Bournaud, F., Charlot, S., et al. 2014, ApJ

Kennicutt, R. C. 1998, A&AS, 36, 189

Kennicutt, R. C., & Evans, N. J. 2012, ARA&A, 50, 531

Kümmel, M., Walsh, J. R., Pirzkal, N., Kuntschner, H., & Pasquali, A. 2009, PASP, 121, 59

Lada, C. J., & Lada, E. A. 2003, ARA&A, 41, 57

Lewis, A., & Bridle, S. 2002, physics review, 66

NASA. 2014, Beyond Our Solar System: Overview

Osterbrock, D. E., & Ferland, G. J. 2006, Astrophysics of Gaseous Nebulae and Active Galactic Nuclei, 2nd edn. (University Science Books)

Searle, L., Sargent, W. L. W., & Bagnuolo, W. G. 1973, ApJ, 179, 427

Tinsley, B. M. 1968, ApJ, 151, 547

Whitaker, K. E., van Dokkum, P. G., Brammer, G., & Franx, M. 2012, The Astrophysical Journal Letters, 754, 6

Zeimann, G., Gebhardt, H., Ciardullo, R., Gronwall, C., & Hagen, A. 2014, American Astronomical Society

Academic Vita

Can Cui

Phone: (814)-954-2229
Email: xdfcuican@gmail.com
Address: 1422 N Allen Street, State College, PA 16803

EDUCATION

The Pennsylvania State University, University Park — May 2014
Schreyer Honors College

- Major: Astronomy (B.S.) and Physics (B.S.)
- Minor: Mathematics
- Dean's List: 8/8 semesters

RESEARCH EXPERIENCE

Research Assistant — Feb 2012—May 2013
Penn State Hobby-Eberly Telescope Dark Energy Experiment (HETDEX)
The Pennsylvania State University, University Park, PA

- Participated as an active member in Prof. Robin Ciardullo's HETDEX research group.
- Assisted with data preparation of the Hobby-Eberly Telescope Dark Energy Experiment.
- Measured Luminosities and equivalent widths for Lyman-alpha emitting galaxies.

Honors Thesis Project (In progress) — July 2013—Present
The Pennsylvania State University, University Park, PA

- Reduced Hubble Space Telescope Advanced Camera for Surveys (ACS) slitless spectroscopic data from 3D-HST;identifield and classified galaxies of interest.
- Selected a sample of emission-line galaxies to compare with more local galaxies to test models of galactic chemical evolution.
- Working toward defining the evolution of fundamental metallicity relation of the selected galaxies.
- Aim to measure star formation rate, stellar mass, extinction, and oxygen abundance.

HONORS

- Dean's List every semester — Fall 2010—Present
- Elsbach Honors Scholarship — Fall 2012— Spring 2014
- Member of Golden Key International Honor Society. — Spring 2011— Present
- Member of Sigma Pi Sigma – The Physics Honor Society — Spring 2011—Present

PROGRAMMING SKILLS

Python; IDL; Mathematica; C++

MISCELLANEOUS

- Native in Mandarin and fluent in English.
- Interested in Piano.